RSC Advances

PAPER

View Article Online
View Journal | View Issue

Cite this: *RSC Adv.*, 2014, **4**, 60280

Zinc, copper and nickel derivatives of 2-[2-bromoethyliminomethyl]phenol as topoisomerase inhibitors exhibiting anti-proliferative and anti-metastatic properties†

Sze Koon Lee,[a] Kong Wai Tan*[a] and Seik Weng Ng[ab]

Received 26th August 2014
Accepted 4th November 2014

DOI: 10.1039/c4ra09256b

www.rsc.org/advances

Three transition metal derivatives of (2-[2-bromoethyliminomethyl]phenol), M[$OC_6H_4CH{=}NCH_2CH_2Br]_2$ (M is zinc, copper and nickel) along with $Ni[OC_6H_4CH{=}NCH_2CH_2]_2(H_2O)_4{\cdot}2Br$, were found to inhibit topoisomerase I (topo I) activity, induce DNA cleavage and bind to calf thymus DNA. The compounds were found to be cytotoxic when tested against cancer cell lines (A2780, MCF-7, HT29, HepG2, A549, PC3, LNCaP), and were anti-invasive against PC3. The inhibitory strength of the metal complexes was higher than that of the organic compound. The neutral metal complexes were synthesized by the reaction of the metal acetates with the Schiff base ligand whereas the bromide salt was obtained upon recrystallization of the nickel derivative from water. In the crystal structure of this salt, the cyclized Schiff base ligand binds to the nickel atom through its nitrogen donor, the metal atom showing an all-*trans* octahedral geometry. The metal atom in $Cu[OC_6H_4CH{=}NCH_2CH_2Br]_2$ exists in a square-planar environment.

1. Introduction

Camptothecin and its analogs target topoisomerase I,[1] their activity being significantly augmented upon complexation with metal ions.[2,3] Researchers have addressed this issue of metal-based drugs by using Schiff base complexes of zinc and copper;[4–7] for example, Desideri and co-workers have proposed that the oxindole-Schiff base complexes inhibit topo I activity through the interaction with amino acid residues at the catalytic site of topo I.[6] Although other studies have explored the potential of Schiff base complexes, by focusing on DNA interaction and cytotoxicity, topo I inhibition is generally not examined.[8–11]

Recently, two studies suggested that the corresponding derivatives of thiosemicarbazones and hydrazones exhibit such behavior towards prostate cancer cells (PC3);[7,12] the activity appears to be enhanced with the introduction of a bromoethyl group,[13] the reason being attributed to the ability of the unit to alkylate the guanine residues in DNA.[14,15] Support for this is provided by Barton and co-workers, who found that a rhodium intercalator tethered to an alkylating agent could selectively alkylate mismatched DNA.[16]

With the above objectives in mind, we are reporting the syntheses and characterization of $[Zn(\mathbf{L1})_2]$ (**1**), $[Cu(\mathbf{L1})_2]$ (**2**), $[Ni(\mathbf{L1})_2]$ (**3**), and $[Ni(\mathbf{L1^C})_2]$ (**4**) complexes (where $\mathbf{L1^C}$ is the self-cyclized **L1** ligand) of bromoethyl containing Schiff base (**L1**), as well as their interaction with DNA and topoisomerase I, cytotoxic and anti-invasion activities against the backdrop of their crystal structures.

2. Results and discussion

2.1 Crystal structure of $Cu[OC_6H_4CH{=}NCH_2CH_2Br]_2$

The crystal data and selected bond lengths and angles were presented in Tables S1 and S2† respectively. The metal atom in $Cu[OC_6H_4CH{=}NCH_2CH_2Br]_2$ (Fig. 1) is coordinated by two phenolate oxygen atoms and two imine nitrogen atoms in an all-*trans* square planar geometry. The Cu–O and Cu–N distances [1.896 (2) Å and 2.008 (2) Å] are in good agreement with the bond distances found in other similar Schiff base complexes.[17,18] Molecules are stacked in a herringbone arrangement along the *a* axis (Fig. 2a) and packed in a parallel fashion in the *b* projection (Fig. 2b).

2.2 Spectroscopic measurements of L1 and complexes 1–4

An intense band was observed in the range of 771–746 cm^{-1} in the IR spectra of **L1** and complexes **1–3**, which is ascribed to the ν(C–Br). Meanwhile, the ν(C=N) of the azomethine group in

[a]*Department of Chemistry, University of Malaya, 50603, Kuala Lumpur, Malaysia. E-mail: kongwai@um.edu.my*

[b]*Chemistry Department, Faculty of Science, King Abdulaziz University, P. O. Box 80203, Jeddah, Saudi Arabia*

† Electronic supplementary information (ESI) available. CCDC 1007051 and 1007052. For ESI and crystallographic data in CIF or other electronic format see DOI: 10.1039/c4ra09256b

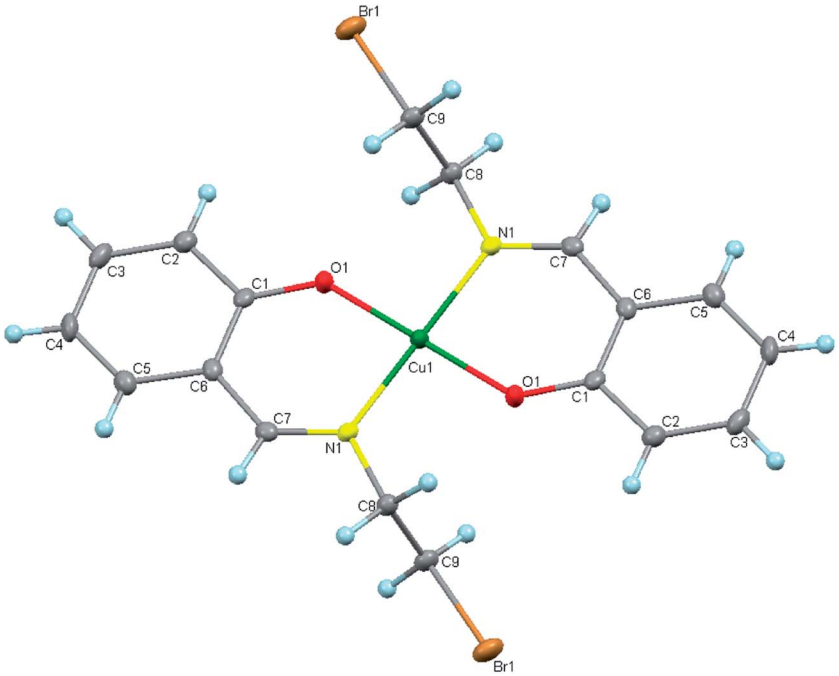

Fig. 1 Thermal ellipsoid plot of complex **2** is drawn at 50% probability level. Hydrogen atoms are drawn at arbitrary radii.

complexes **1–4** was shifted towards lower frequencies (1620–1606 cm^{-1}), indicating the coordination of imine nitrogen atom to the metal ions.[19,20] Besides that, the IR spectrum of complex **4** showed a sharp band at 3298 cm^{-1} assigned to the ν(OH) of coordinated water molecules.

Electronic spectra of **L1** and complexes **1–4** were recorded in DMSO in the region of 220–500 nm at room temperature. An intense absorption band at about 240–252 nm was observed in **L1** and complexes **1–4** associated with the benzene ring π–π^* transition.[21] Besides that, Schiff base ligand **L1** has a characteristic absorption band at 397 nm ($\varepsilon = 4.83 \times 10^3$ M^{-1} cm^{-1}) due to the π–π^* transition of imine.[22] Upon complexation, the absorption band of imine of complexes **2–4** has shifted to 373 nm ($\varepsilon = 9.08 \times 10^3$ M^{-1} cm^{-1}), 361 nm ($\varepsilon = 1.05 \times 10^4$ M^{-1} cm^{-1}), and 309 nm ($\varepsilon = 2.74 \times 10^3$ M^{-1} cm^{-1}) respectively, while the position of imine band of complex **1** remain unchanged at 397 nm ($\varepsilon = 4.52 \times 10^3$ M^{-1} cm^{-1}). In addition, a broad band at 675 nm and 614 nm was observed for complex **2** and complex **3** respectively, which were assigned to the d–d transition. However, no d–d band was observed for complex **4**.

A characteristic peak assigned to the azomethine hydrogen at 8.3 ppm was observed, which confirmed the formation of Schiff base ligand **L1**. Aromatic protons of salicylaldehyde were present in the range of 6.88–7.48 ppm. The coordination of azomethine nitrogen to metal ion was supported by upfield shifting of CH=N peak from 8.58 ppm in **L1** to 8.30 ppm in the spectrum of complex **1**.[23,24] In addition, the disappearance of the phenolic proton in the spectrum of complex **1** suggested the complexation of the ligand to metal ion *via* phenolate oxygen.

2.3 The reaction of complex 3 to form complex 4

Yet, what is particularly tantalizing is that the stirring of complex **3** in hot aqueous solution has catalyzed the self-cyclization of Schiff base ligand **L1** to obtain complex **4** with a seven-membered rings ligand (2,3-dihydro-1,4-benzoxazepine, $\mathbf{L1^C}$) through Williamson ether reaction as shown in Fig. 3.[25,26] However, the desired product could not be produced for complexes **1** and **2**. It is plausible that the self-cyclization of **L1** is catalyzed by the Ni(II) ions in the base free reaction. Similar observation was reported by Saha *et al.* recently in the synthesis of Ni(II) complex of 9-methoxy-2,3-dihydro-1,4-benzoxyzepine, carried out in a different reaction condition.[27] The conversion of **L1** to $\mathbf{L1^C}$ under such condition is notable as it involves green chemistry, achieves considerable yield, and relatively simple as compared to other reported methods.[28–31]

2.4 Crystal structure of complex 4

The crystal data of complex **4** was tabulated in Table S1.† Complex **4** crystallized in a monoclinic system and showed distorted octahedral environment since the angles of O1W–Ni1–O2W, N1–Ni1–O1W, and N1–Ni1–O2W are deviated from the ideal 90°. The nickel atom is ligated by two imine nitrogen atoms of two $\mathbf{L1^C}$ and four oxygen atoms of four water molecules (Fig. 4). Complex **4** is accompanied by two bromide anions due to its cationic nature. Both the coordinated $\mathbf{L1^C}$ are not planar due to the folding of seven-membered rings with O1, C8, and C9 out of the plane. The dihedral angles between the aromatic rings with C8–C9–N1 and O1–C7–C8 are 46.63° and 20.29° respectively. In addition, both the $\mathbf{L1^C}$ are *trans* to each other (N1–Ni1–N1 = 180°),[32,33] the $\mathbf{L1^C}$ ligands are in the apical positions and four water molecules lie in the equatorial plane.

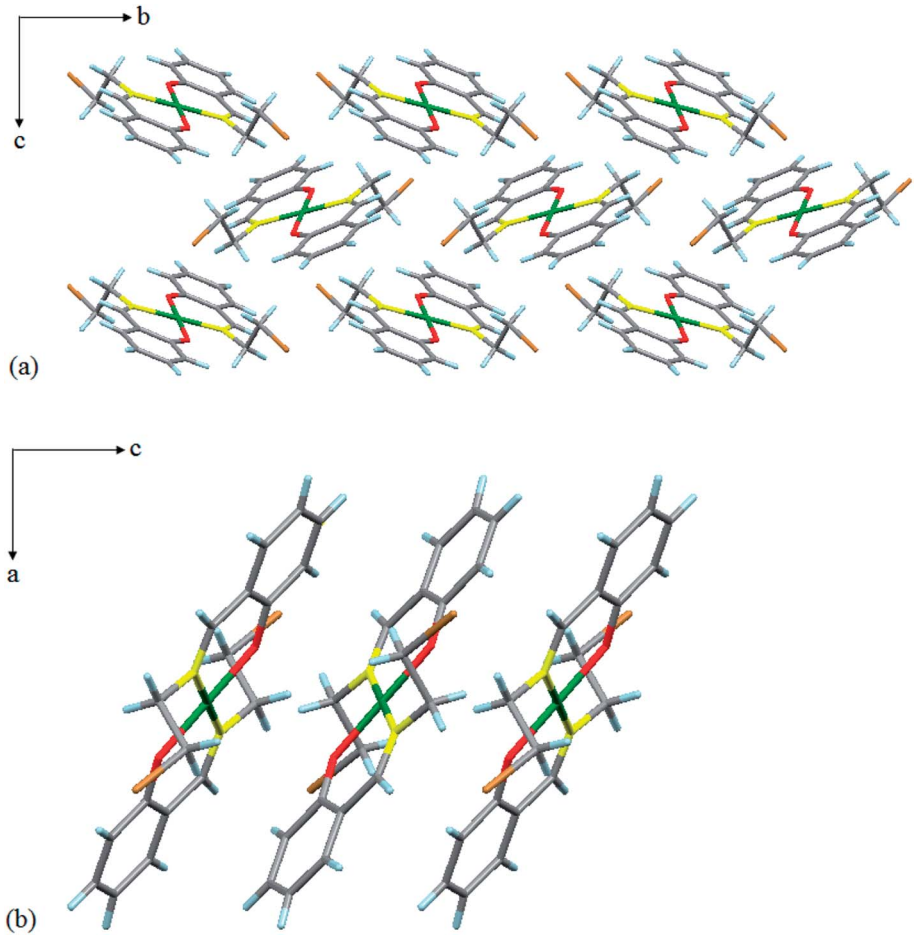

Fig. 2 (a) The herringbone arrangement of complex **2** along the *a* axis. (b) The parallel packing of complex **2** in the *b* projection. Green = Cu, red = O, yellow = N, brown = Br, grey = C, and blue = H.

The bond lengths of Ni1–N1, Ni1–O1W, and Ni1–O2W are 2.0778 (18) Å, 2.0790 (18) Å, and 2.0879 (18) Å respectively, are matched well with the literature values[27] (Table S2†).

The packing of the molecules of complex **4** is presented in Fig. 5. The aromatic rings are stacked in a herringbone fashion along the *a* axis. The distances of hydrogen bonding of complex **4** are shown in Table S3.† The molecules in the crystal lattice are stabilized by zigzag hydrogen bonding chains in *b* projection (Fig. 5c), a bromide anion is H-bonded with four H atoms of the coordinated water molecules (O1W–H11···Br1, O1W–H12···Br1, O2W–H21···Br1, and O2W–H21···Br1) and is responsible for the stacking arrangement (Fig. 5b).

2.5 Topoisomerase I inhibition assay

Complexes **1–3** inhibited the topo I activity in a dose dependent manner while **L1** and complex **4** were found to be inactive as shown in Fig. 6. Complexation of **L1** has enhanced the topo I inhibition effect.[2–4,7,13] Cu(II) complex **2** was the most active complex in this series, since partial inhibition of topo I activity was induced at 10 μM and total inhibition was observed at 80 μM. On the other hand, Zn(II) complex **1** and Ni(II) complex **3** required a higher concentration, 250 μM and 500 μM respectively to induce slight inhibition of topo I activity. No complete inhibition was detected for complexes **1** and **3**. The appearance of DNA laddering in the gel suggested that complexes **1–3** may

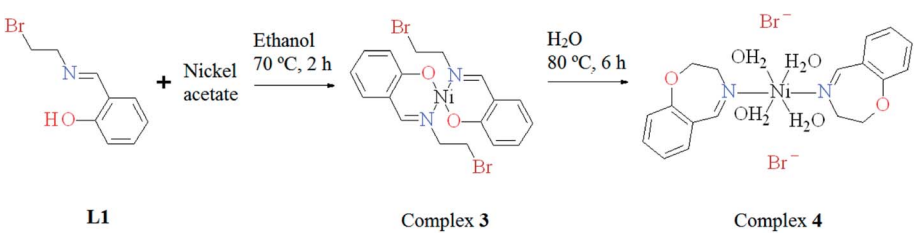

L1 Complex **3** Complex **4**

Fig. 3 Synthesis route of complex **4**.

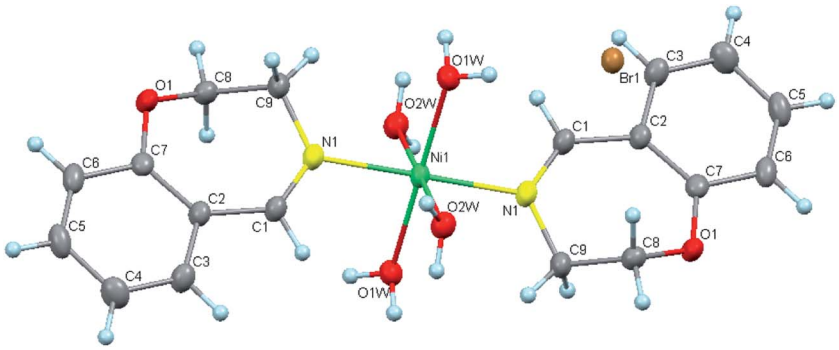

Fig. 4 Thermal ellipsoid plot of complex **4** is drawn at 50% probability level. Hydrogen atoms are drawn at arbitrary radii.

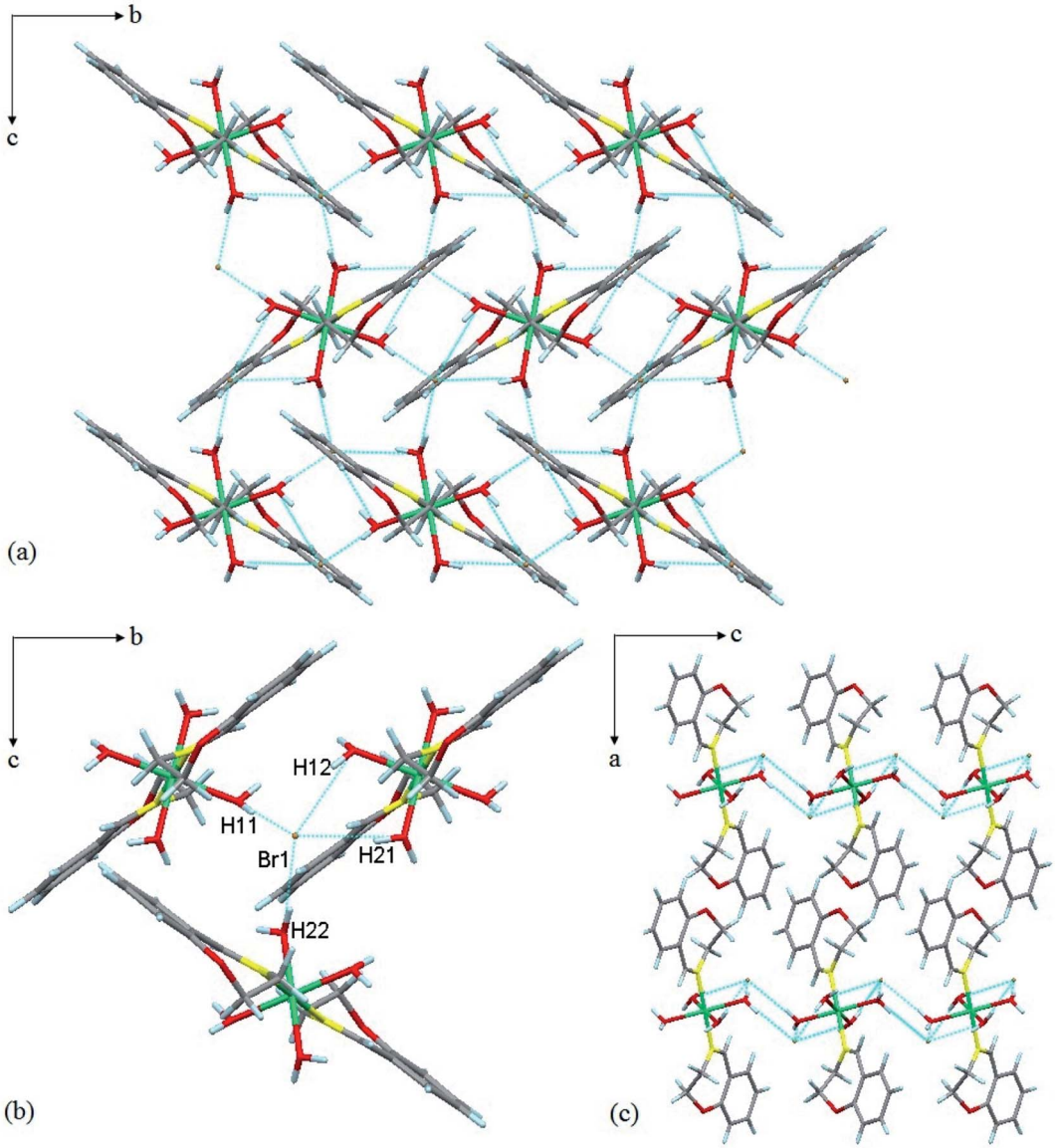

Fig. 5 (a) The herringbone packing of complex **4** in the *a* projection. (b) Hydrogen bonding between the water molecules and bromide anion. (c) The packing and hydrogen bonding pattern of complex **4** along the *b* axis. Blue dotted lines represent hydrogen bonding. Green = Ni, red = O, yellow = N, brown = Br, grey = C, and blue = H.

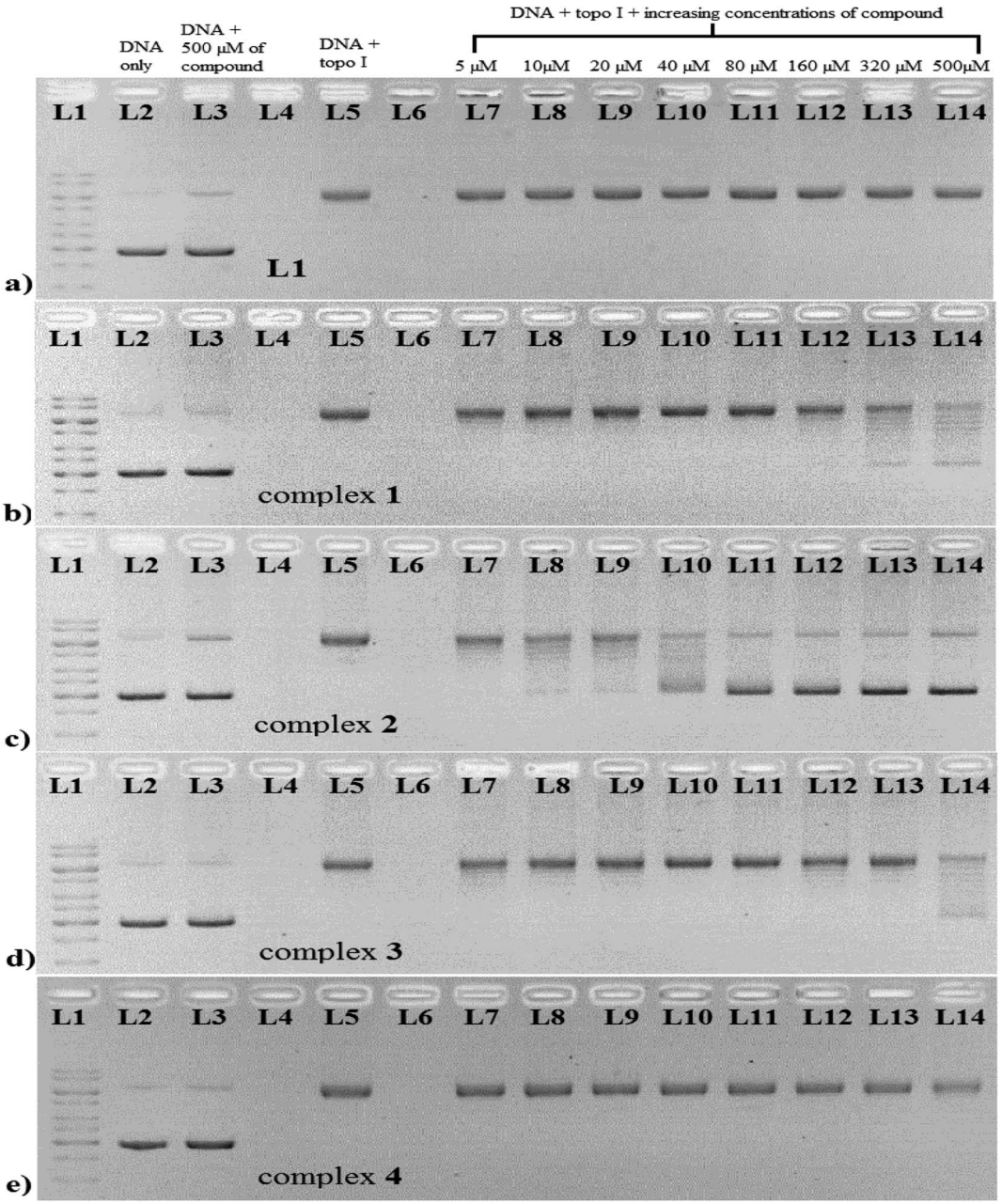

Fig. 6 Electrophoresis result of incubating *E. coli* topo I (0.25 unit/20 μl) with pBR322 in the absence and presence of various concentrations (5–500 μM) of **L1** (a), **1** (b), **2** (c), **3** (d), and **4** (e). Lane 1, Gene Ruler™ 1 kb DNA ladder; lane 2, DNA alone; lane 3, DNA + 500 μM of **L1** or **1–4**; lane 5, DNA + 0.25 unit *E. coli* topo I; lane 7–14, DNA + 0.25 unit *E. coli* topo I + increasing concentrations of **L1** or **1–4** (5 μM, 10 μM, 20 μM, 40 μM, 80 μM, 160 μM, 250 μM, and 500 μM respectively).

act as topo I poisons by stabilizing the DNA-topo I cleavage complex.[5] The inhibitory strength of these compounds was found to follow the order: **2 > 1 > 3 > 4 ≈ L1.**

According to Desideri *et al.*, oxindolimine Zn(II) and Cu(II) complexes could inhibit topo I activity, with the Cu(II) complex being more active than the Zn(II). The molecular docking study showed that this difference is due to the different coordination geometry of the complexes. The square planar Cu(II) complex formed a stable complex with amino acid residues of topo I in one of the two "lips" that clamp DNA during the cleavage reaction, whereas the more tetrahedral Zn(II) complex only allowed a loose interaction with topo I.[6] This may also explains why the octahedral complex **4** with non-planar ligands is inactive in inhibiting topo I activity.

2.6 Nucleolytic study

We observed that the **L1** exhibits comparable DNA cleavage activity with its metal complexes in the absence of external agent at neutral pH, while metal chloride alone has a negligible effect on DNA cleavage as shown in Fig. 7. Schiff base ligand **L1**

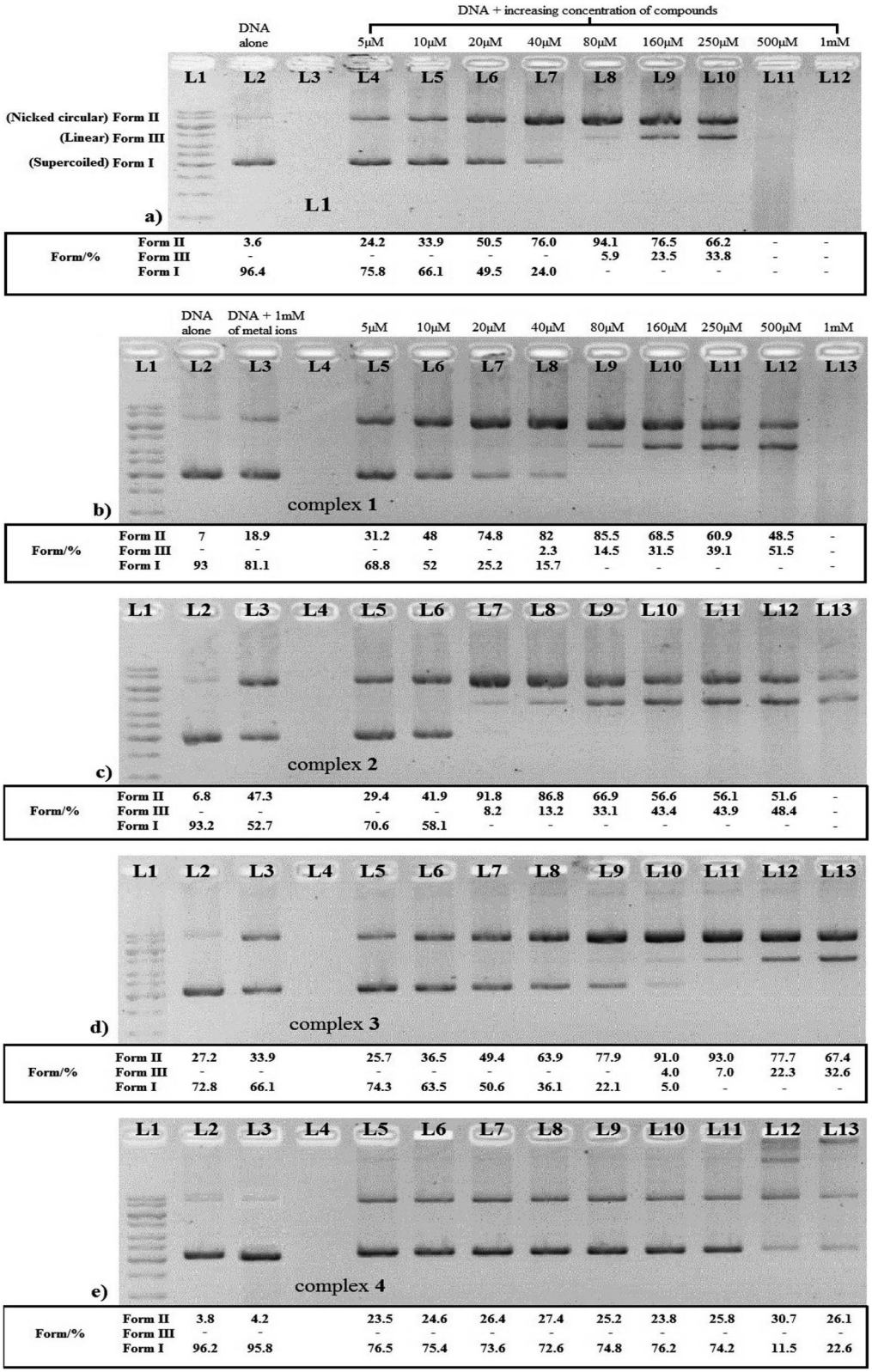

Fig. 7 Electrophoresis result of incubating pBR322 with **L1** (a), **1** (b), **2** (c), **3** (d), and **4** (e) in TN buffer (5 mM Tris, 50 mM NaCl) pH 7.5 at 37 °C for 48 h. Lane 1, Gene Ruler™ 1 kb DNA ladder; lane 2, DNA alone; lane 3 (b–e), DNA + 1 mM MCl_2 (M = Zn, Cu, Ni); lane 4–12 (a), DNA + increasing concentrations of **L1** (5 μM to 1 mM); lane 5–13 (b–e), DNA + increasing concentrations of **1–4** (5 μM to 1 mM respectively).

and complexes **1–3** started to induce double-stranded DNA scission with different concentration of 80 μM, 40 μM, 20 μM, and 160 μM respectively. In addition, **L1**, complexes **1** and **2** were able to cut linear DNA into smaller fragments that cannot be quantified at 500 μM to 1 mM, causing smearing and fading of DNA bands. On the other hand, complex **4** was a relatively weaker but site specific nucleolytic agent as it catalyzed the cleavage reaction and produced 23.5–27.4% of nicked DNA at a variety of concentrations (5–250 μM), and restrained the migration of DNA across the gel starting from 500 μM; suggestive of binding of complex **4** to DNA forming DNA aggregates. This might be due to the difference in structure and coordination geometry of complex **4**. Result showed that these compounds cleaved DNA by the following order: **2** > **1** > **L1** > **3** > **4** based on their ability to catalyze the cleavage reaction to produce linear DNA at 80 μM.

It is not surprising that Schiff base ligand **L1** can perform DNA scission. There are several studies reporting better DNA cleavage activity of the free ligand than its Co(II) and Zn(II), Cu(II), and Ni(II) complexes.[34–36] The phenyl ring of **L1** may intercalate into DNA, while the hydroxyl group acts as a nucleophilic group in the transphosphorylation reaction.[34,36–39] Nevertheless, the significant DNA cleavage activity induced by **L1** is probably due to its smaller molecular size and lack of any site specificity as compared to its tetra-coordinated metal complexes. The DNA cleavage activity of complexes **1–3** is reminiscent of the Schiff base **L1**, demonstrating the role of ligand in the DNA cleavage mechanism.

Even though the DNA cleavage reaction of Cu(II) and Ni(II) complexes **2–4** does not require external agent, the possibility that DNA cleavage occurs *via* the production of reactive oxygen species (ROS) need to be discounted; so mechanistic study using scavengers of hydroxyl radical (DMSO and thiourea), singlet oxygen radical (sodium azide), and superoxide anion (tiron), and a Cu(I) specific chelator (neocuprione) were carried out (Fig. S1†). For Cu(II) complex **2**, the addition of neocuprione had partially inhibited the DNA cleavage; with the retainment of supercoiled DNA (40.1%). Moreover, thiourea, sodium azide, and DMSO reduced the conversion of nicked DNA to linear DNA by 8–10%. All of the above results corroborated a self-activating mechanism for complex **2**; whereby the redox-active Cu(II) center is initially reduced to Cu(I), and subsequently reacts with dioxygen to produce hydroxyl and singlet oxygen radicals that cause the DNA breaks,[40,41] thus, the involvement of oxidative pathway in the cleavage reaction catalyzed by complex **2** cannot be ruled out. However, a rare phenomenon was observed where the addition of tiron enhanced the DNA cleavage activity by producing 49.1% linear DNA, the exact reason is still under investigation and similar observation has been reported by Seng *et al.*[42] Furthermore, thiourea caused smearing above the nicked DNA band that contains a variety of DNA conformations, which might be due to the binding of complex **2** on the partially-catalyzed cleaved residues of nicked DNA. On the other hand, all of the tested radical scavengers have no obvious effect on the extent of DNA cleavage by Ni(II) complexes **3** and **4**. It is not uncommon for Cu(II) and Ni(II) complexes to carry out DNA cleavage in the absence of external agent.[43,44]

2.7 DNA binding study

The absorption spectra of **L1** and complex **1** incubated with increasing CT-DNA concentrations are shown in Fig. 8, while the absorption spectra of complexes **2–4** are shown in Fig. S2.† Schiff base ligand **L1** and complexes **1–3** exhibited different degree of hypochromism at 361–397 nm, accompanied by a blue shift as tabulated in Table 1. Besides that, slight hyperchomism at ~320 nm and the appearance of an isobestic point at 330–350 nm upon the addition of CT-DNA for **L1**, complexes **1** and **3** suggested the existence of an equilibrium between the free compound and CT-DNA bound compound. On the other hand, complex **4** showed modest hypochromism (5.79%) at 309 nm. The observed hypochromism and blue shift may be an evidence of non-covalent interaction between the compounds and DNA; probably *via* intercalation.[45–48]

Complex **1** exhibits highest K_b value (3.62×10^7), followed by **L1** (1.07×10^7), **4** (6.68×10^6), **3** (5.22×10^6), and **2** (8.20×10^5). The K_b values of **L1** and complexes **1–4** are comparable to classical intercalator ethidium bromide (1.4×10^6 M^{-1})[49] and metallointercalator $[Ru(bpy)_2(dppz)]^{2+}$, bpy = 2,2′-bipyridine, dppz = dipyridol[3,2-*a*:2′,3′-*c*]phenazine (>10^6 M^{-1}).[50,51] Furthermore, similar trend was observed in the interaction of metallopyrazoliumylporphyrins with CT-DNA, the K_b values followed the trend Zn > Ni > Cu, probably due to different interaction mode and preferential DNA-sequence affinity.[52,53]

2.8 Cytotoxicity study

The cytotoxic activity of Schiff base ligand **L1** and complexes **1–4** against various human cancer cell lines such as A2780, MCF-7, HT29, HepG2, A549, PC3, and LNCaP were evaluated by MTT assay and presented in Table 2. Cultured cancer cells were treated with compounds and incubated for 24 h and the IC_{50} values were determined from the plots of cancer cells survival against increasing concentration of tested compounds as shown in Fig. S3 and S4.† Cisplatin was used as a positive control. Schiff base ligand **L1** and complex **4** were inactive in all the cell lines tested, whereas complex **3** was relatively less cytotoxic to cancer cells than complexes **1** and **2**. The complexation of **L1** with Zn(II) and Cu(II) metal ions greatly enhanced its cytotoxic activity. Zn(II) complex **1** displayed significant cytotoxic activity towards PC3 and LNCaP cells (<15 μM), while Cu(II) complex **2** was highly toxic against HT29, HepG2, PC3, and LNCaP (<20 μM). It is not astonishing that complex **1** exerts prominent cytotoxic activity against prostate cancer cells because human prostate epithelial cells are shown to uniquely accumulate high level of zinc and consequently induce apoptotic cell death.[54,55]

Moreover, this finding is consistent with the result from topo I inhibition study as shown in Fig. 6. The level of topo I is often overexpressed in colon, lung, and prostate cancers.[56] Complex **2** being the most active topo I inhibitor in this series also exhibits remarkable cytotoxic activity against these cancer cell lines, which proposed that complexes **1–3** induced cytotoxicity by inhibiting topo I activity.

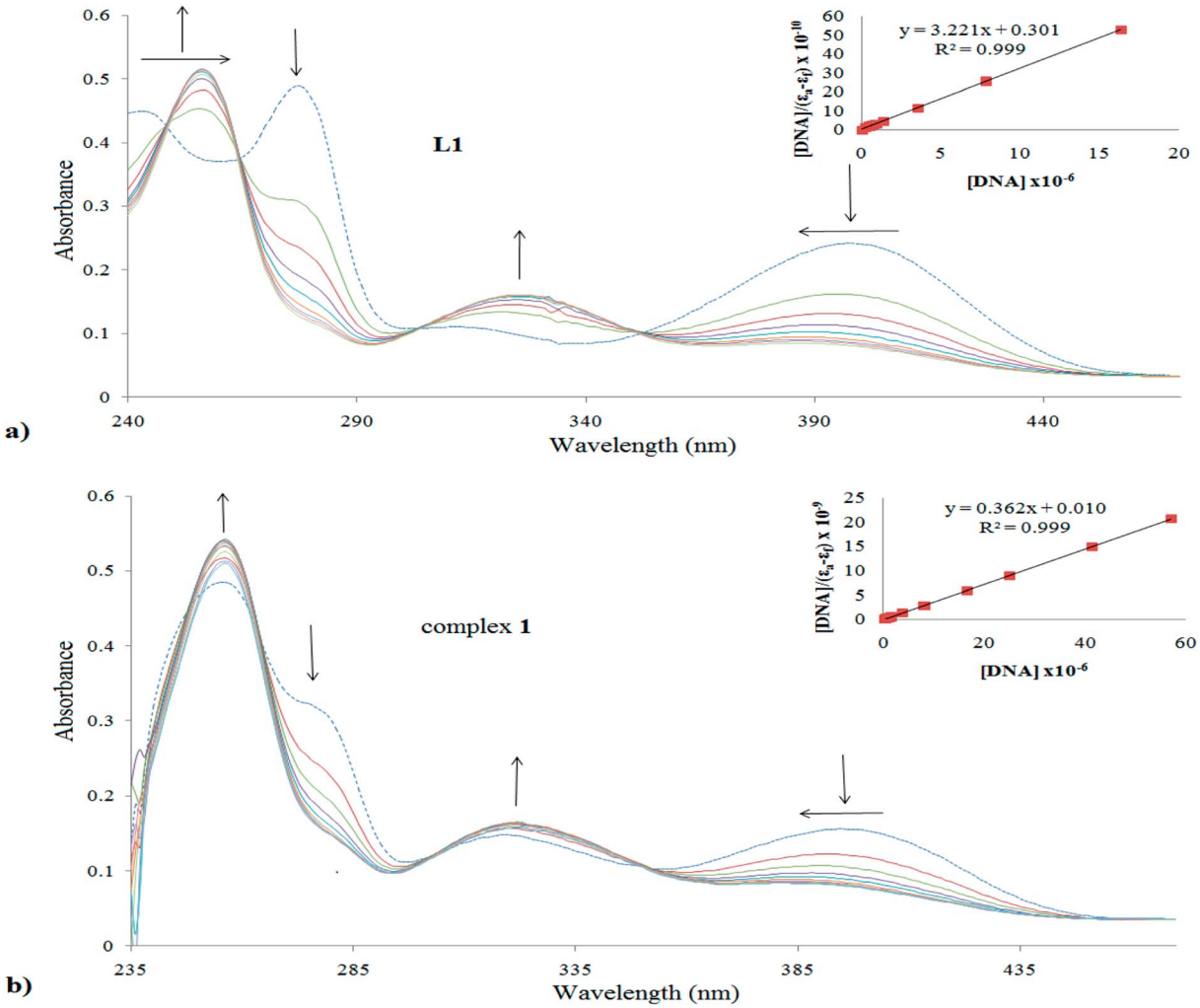

Fig. 8 UV-Vis absorption spectra of **L1** (a) and **1** (b) in TN buffer pH 7.5, in the absence (dashed line) and presence (solid line) of CT-DNA with increasing concentrations. Arrows show the change in absorbance with increasing DNA concentration. The insets represent the K_b calculation plots for the spectra changes at 397 nm of **L1** and complex **1**.

2.9 Cell invasion study

The metastasis of cancer cells to remote sites is the major cause of cancer death.[57,58] Cancer cells will need to degrade the basement membrane before they spread and invade through the body. Therefore, the cell invasion assay employs the protein complex Matrigel, which simulates the *in vivo* cellular basement membrane and demonstrates the anti-invasive activity of compounds by keeping the cancer cells localized. The lesser the number of cancer cells migrate through the Matrigel, the greater the ability of compound to prevent the invasion of cells.[59] Since most of the tested compounds were active against prostate cancer, we decided to study the anti-invasive activity of these compounds on the more invasive PC3 cancer cells.[60,61] The result obtained from the study was depicted in Fig. 9 and 10.

The invasion rates of PC3 cells after treated with cisplatin and complexes **1–4** were 47.79 ± 16.62%, 24.87 ± 8.33%, 14.97 ± 13.32%, and 7.78 ± 9.54%, and 80.86 ± 18.18% respectively

Table 1 Spectral features of the UV spectra of **L1** and complexes **1–4** upon addition of CT-DNA

Compound	λ (nm)	Change in absorbance	Isobestic point (nm)	Red shift (nm)	Blue shift (nm)	Hypo (%)	K_b (M^{-1})
L1	397	Hypochromism	352	—	19	64.65	1.07×10^7
1	397	Hypochromism	351	—	14	62.83	3.62×10^7
2	373	Hypochromism	—	—	21	46.61	8.20×10^5
3	361	Hypochromism	335	—	5	51.08	5.22×10^6
4	309	Hypochromism	—	—	—	5.79	6.68×10^6

Table 2 Cytotoxic activity of Schiff base **L1** and its metal complexes **1–4** against several cancer cell lines after 24 h treatment

	IC_{50} (μM)						
	A2780	MCF-7	HT29	HepG2	A549	PC3	LNCaP
Compound	Ovarian cancer	Breast cancer	Colon cancer	Hepatocellular carcinoma	Lung carcinoma	Prostate carcinoma	
Cisplatin	28.80	19.60	25.00	152.00	35.40	271.50	32.53
L1	>80	>80	>80	>80	>80	>80	>80
1	68.97	26.77	32.83	67.60	>80	14.93	13.60
2	70.70	25.77	14.07	18.47	29.43	17.37	14.10
3	>80	>80	68.02	>80	61.77	57.77	41.70
4	>80	>80	>80	>80	>80	>80	>80

(invasion rates are normalized over the control). Notably, complexes **1–3** were quite effective anti-invasive agents as compared to complex **4** and cisplatin. Counterintuitively, the less cytotoxic complex **3** has created a greater obstacle for the invading cells than the more cytotoxic complexes **1** and **2**. It is not surprising as the ruthenium compound, imidazolium *trans*-imidazoledimethyl sulfoxydetetrachloro-ruthenate (NAMI-A) also shows similar characteristics.[62,63] Based on the result obtained, it was proposed that the Ni(II) complex exhibits better anti-invasion activity against PC3 cells than its Zn(II) and Cu(II) analogs, but the absence of bromoalkyl group significantly reduced the activity as shown by Ni(II) complex **4**. Recently, Radulovic and colleague showed a rare example of Ni(II) complex of selenosemicarbazones that could inhibit the invasion of human breast cancer MDA-MB-361 cells more effectively than the Cd(II) and Zn(II) complexes.[64]

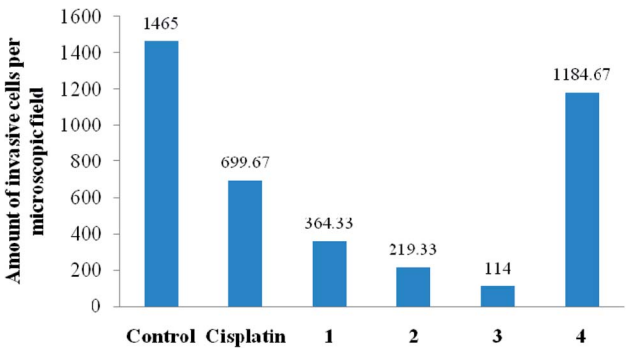

Fig. 10 Cell invasion assay result of cisplatin and complexes **1–4** against PC3.

3. Experimental

3.1 Materials and solutions

The chemicals for syntheses were bought from Sigma and solvents were purchased from Merck. The pBR322, gene ruler 1 kb DNA ladder, 6× loading buffer, were purchased from BioSyn Tech (Fermentas). Analytical grade agarose powder was bought from Promega. *E. coli* topoisomerase I was purchased from New England Biolabs. Calf-thymus DNA (CT-DNA), sodium chloride, and ethidium bromide were bought from Sigma Chemical Co. (USA). All solutions for DNA experiments were prepared with ultra-pure water from an Elga PURELAB ULTRA Bioscience water purification system with UV light accessory. Tris–NaCl (TN) buffer was prepared from the combination of Tris base and NaCl dissolved in aqueous

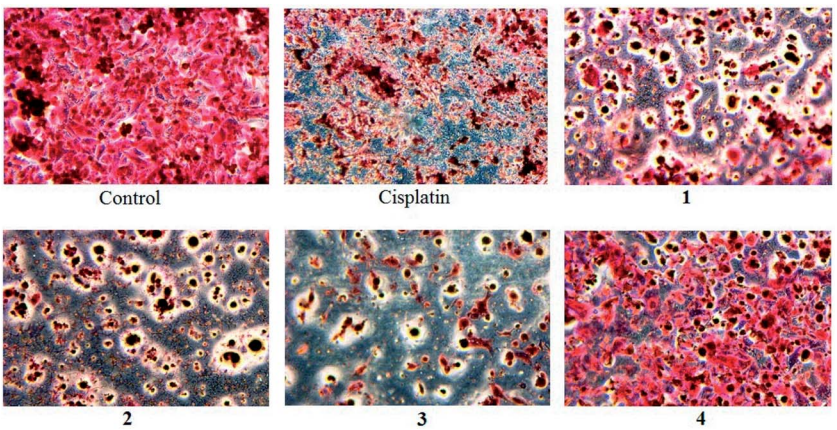

Fig. 9 Microscope images of invading PC3 cells that have migrated through the Matrigel: The extent of inhibition of cell invasion by cisplatin and complexes **1–4** against PC3 cells can be seen from the decrease in the numbers of invading cells.

solution. The pH of TN buffer was adjusted with hydrochloric acid solution until pH 7.5, which contains Tris at 5 mM and NaCl at 50 mM. All the tested compounds were freshly prepared daily.

3.2 Physical measurements

IR spectra were recorded as KBr pellets by using a Perkin-Elmer Spectrum RX-1 spectrometer. NMR spectra were recorded in deuterated DMSO-d on a JEOL JNM-LA400 or ECA 400 MHz instrument. Elemental analyses were carried out on a Thermo Finnigan Eager 300 CHNS elemental analyzer. UV-Vis spectroscopic measurements were performed on a Shimadzu UV-1650 PC spectrophotometer.

3.3 Syntheses

3.3.1 Synthesis of 2-[2-bromoethyliminomethyl]phenol (L1). The Schiff base ligand **L1** was synthesized according to the method described by Grivani *et al.* with minor modification.[20] Rapid evaporation of the solvent yielded yellow needle crystals in high yield. The crystals were filtered, washed with water, dried in the air, and kept in a desiccator over silica gel.

(Yield: 1.87 g, 82%). Anal. calc. for $C_9H_{10}BrNO$: C, 47.4; H, 4.4; N, 6.1. Found: C, 47.2; H, 4.3; N, 6.3%. IR (KBr disc, cm^{-1}): 3005 w, 2883 m, 2832 w, 2725 w, 2654 w, 1630 s (C═N), 1498 m, 1429 m, 1277 s, 1264 s, 1056 s, 841 s, 760 s (C–Br), 639 m, 560 m, 454 m (s, strong; m, medium; w, weak).

Characteristic ^{1}H NMR signals (DMSO-d_6, TMS, s, singlet; d, doublet; m, multiplet) δ (ppm): 13.21 (s, 1H, O–H), 8.58 (s, 1H, H–C═N), 6.88–7.48 (m, 4H, C–H, phenyl), 4.00 (d, 2H, N–CH_2–), and 3.80 (d, 2H, –CH_2Br).

3.3.2 Synthesis of $[Zn(L1)_2]$ (1). L1 (0.46 g, 2 mmol) was added dropwise into an ethanolic solution of zinc acetate (0.22 g, 1 mmol) and refluxed for 2 h. Yellow precipitates formed were filtered, washed with ethanol and water, dried in the air, and kept in a desiccator over silica gel.

(Yield: 0.31 g, 68%). Anal. calc. for $C_{18}H_{20}Br_2N_2O_2Zn$: C, 41.5; H, 3.9; N, 5.4%. Found: C, 41.6; H, 3.3; N, 5.5. IR (KBr disc, cm^{-1}): 3435 w, 3032 w, 2955 w, 1620 s (C═N), 1537 s, 1467 m, 1450 m, 1324 m, 1189 m, 1148 m, 757 m (C–Br), 598 w, 465 w, 450 w (s, strong; m, medium; w, weak).

Characteristic ^{1}H NMR signals (DMSO-d_6, TMS, s, singlet; d, doublet; m, multiplet) δ (ppm): 8.3 (s, 2H, H–C═N), 6.88–7.48 (m, 8H, C–H, phenyl), 4.00 (d, 4H, N–CH_2–), and 3.81 (d, 4H, –CH_2Br).

3.3.3 Synthesis of $[Cu(L1)_2]$ (2). The general procedure for the synthesis is similar to the complex **1** by using copper acetate to replace zinc acetate. Green crystals suitable for X-ray diffraction study were obtained by dissolving the green powders in a mixture of dimethylformamide and ethanol and allowed to evaporate slowly at room temperature.

(Yield: 0.37 g, 72%). Anal. calc. for $C_{18}H_{20}Br_2N_2O_2Cu$: C, 41.6; H, 3.9; N, 5.4%. Found: C, 41.8; H, 3.3; N, 5.3. IR (KBr disc, cm^{-1}): 3024 w, 2908 w, 1611 s (C═N), 1443 s, 1326 s, 1204 m, 1150 m, 908 m, 749 s (C–Br), 733 s, 677 s, 610 m, 577 m, 466 m (s, strong; m, medium; w, weak).

3.3.4 Synthesis of $[Ni(L1)_2]$ (3). The general procedure for the synthesis is similar to the complex **1** by using nickel acetate to replace zinc acetate. Pale green precipitates formed were filtered, washed with water and ethanol, and kept in a desiccators over silica gel.

(Yield: 0.39 g, 75%). Anal. calc. for $C_{18}H_{20}Br_2N_2O_2Ni$: C, 42.0; H, 3.9; N, 5.4%. Found: C, 42.0; H, 3.4; N, 5.4. IR (KBr disc, cm^{-1}): 3437 w, 3029 w, 2935 w, 1610 s (C═N), 1539 s, 1336 m, 1224 m, 1148 m, 917 s, 746 m (C–Br), 733 m, 639 m, 533 m, 462 m, 411 m (s, strong; m, medium; w, weak).

3.3.5 Synthesis of $[Ni(L1^C)_2]$ (4). Complex **3** (0.515 g, 1 mmol) was stirred in 20 ml of hot water and it was slowly dissolved over 6 h. Then, the aqueous solution was concentrated to 5 ml and slow evaporation at room temperature yielded green crystals suitable for X-ray analysis. The green crystals were filtered, washed with diethyl ether and kept in a desiccator over silica gel.

(Yield: 0.362 g, 62%). Anal. calc. for $[(C_9H_9NO)(H_2O)_4Ni]^{2+}\cdot 2Br^-$: C, 37.0; H, 4.5; N, 4.8. Found: C, 37.2; H, 4.4; N, 5.1%. IR (KBr disc, cm^{-1}): 3298 s, 2972 w, 2927 w, 1644 s, 1606 s (C═N), 1564 m, 1491 m, 1273 s, 1181 m, 1128 m, 1060 m, 979 s, 871 w, 771 s (C–Br), 700 w, 661 w, 603 w, 575 w, 509 s (s, strong; m, medium; w, weak).

3.4 X-ray crystallography

The unit cell parameters and the intensity data were collected on a Bruker SMART APEX diffractometer, equipped with a Mo-Kα X-ray source (λ = 0.71073 Å). The APEX2 software was used for data acquisition and the SAINT software for cell refinement and data reduction. Absorption corrections on the data were made using SADABS. The structures were solved and refined by SHELXL97.[65] Molecular graphics were drawn by using XSEED.[66] The structures were solved by direct-methods and refined by a full-matrix least-squares procedure on F^2 with anisotropic displacement parameters for non-hydrogen atoms.†

3.5 *E. coli* topo I inhibition assay

The *E. coli* topo I inhibitory activity was determined by observing the relaxation of supercoiled plasmid DNA, pBR322. The reaction mixtures for this test consisted of 1 × BSA, 10 × NE buffer 4, 0.25 μg of plasmid pBR322, 0.25 units of *E. coli* topo I, and compounds with final concentration of 500 μM. All reactions conducted at a final volume of 20 μl and were prepared on ice. Upon enzyme addition, reaction mixtures were incubated at 37 °C for 30 min. The reactions were terminated by adding 2 μl of 10% sodium dodecyl sulfate (SDS) and followed by 3 μl of 6× loading dye comprising 0.03% bromophenol blue and 60% glycerol. SDS is required to observe a linear DNA fragment and to denature topo I, preventing further functional enzymatic activity. Then, the reaction mixtures were loaded into 1.25% agarose gel and electrophoresed for 3 h at 50 V with running buffer of Tris–acetate–EDTA (TAE) at pH 8.1. The gel was stained, destained, and photographed under UV light using an AlphaImager red® gel documentation system and the digital image was analyzed using Pronto software.

3.6 DNA cleavage experiment

Agarose gel electrophoresis experiments were performed on supercoiled plasmid DNA pBR322 using a horizontal gel system. For the cleavage studies, each 20 μl of sample contained the compound dissolved in buffer, DNA, and the required volume of additional buffer. All samples were incubated at 37 °C in the dark. The reaction mixtures were prepared as follows: 0.5 μl of 50 μM compound or metal salt was added to the mixture of 0.5 μl of plasmid DNA pBR322 (0.25 μg μl^{-1}) and Tris–NaCl buffer at pH 7.5 to give a final volume of 20 μl. The reactions were carried out after incubating the reaction mixtures at 37 °C for 48 h. Next, 3 μl of 6× loading dye was added to the reaction mixtures and electrophoresed at 80 V for 90 min in Tris–acetate–EDTA (TAE) buffer, pH 8.1, using 1.5% agarose gel. Then, the agarose gel was stained with ethidium bromide solution (0.5 μg ml^{-1}). Densitometric quantification of supercoiled DNA and cleavage products after electrophoresis was estimated using TotalLab Quant software.[34,67] Supercoiled plasmid DNA values were corrected by a factor of 1.3 due to the lowered binding of ethidium to this structure.[68–70] To study the DNA cleavage mechanism, several radical scavengers (Tiron, thiourea, DMSO, and sodium azide) and a specific Cu(I) chelator (neocuprione) were used.[42] The reaction mixtures were incubated at 37 °C for 24 h.

3.7 DNA binding study with UV spectroscopy

DNA binding studies have been performed by UV-Vis spectroscopic titration using TN buffer (5 mM Tris; 50 mM NaCl, pH 7.5) at room temperature. Stock solutions of tested compounds were prepared in DMSO and diluted with TN buffer to a concentration of 50 μM as working solutions in the titration experiments. The final concentration of DMSO in the working solution was not more than 10%. DNA stock solution was prepared by dissolving the commercially purchased CT-DNA in TN buffer at 4 °C for 2 days. The purity of the CT-DNA stock solution was checked by comparing the ratio of absorbance at 260 nm and 280 nm. The DNA concentration was determined by the UV absorbance at 260 nm after 1 : 10 dilution using a molar extinction coefficient at 6600 M^{-1} cm^{-1}. CT-DNA stock solution was added gradually into the reaction mixture up to a sufficient concentration for studying. After each addition, the reaction mixture was allowed to incubate for 5 min before the absorption spectrum was recorded. The intrinsic binding constant K_b of tested compounds were calculated by using the Wolfe–Shimmer equation:[71,72]

$$[DNA]/(\varepsilon_a - \varepsilon_f) = [DNA]/(\varepsilon_b - \varepsilon_f) + 1/K_b\,(\varepsilon_b - \varepsilon_f)$$

where ε_a, ε_f, and ε_b correspond to A_{obsd}/[compound], the extinction coefficient for the free compounds, and the extinction coefficient for the compounds fully bound with DNA. In plot of $[DNA]/(\varepsilon_a - \varepsilon_f)$ *versus* [DNA], the intrinsic binding constant K_b is given by the ratio of the slope to *y*-intercept.

3.8 Cytotoxicity assay

Cells used in this study were obtained from American Type Cell Collection (ATCC) and Lonza. These tumour cells were cultured in a RPMI 1640 medium at 37 °C in an atmosphere with 5% CO_2 saturation. *In vitro* cytotoxicity for quantitative evaluation was tested by means of the MTT assay. Cells were seeded at a density of 1×10^5 cells per ml in a 96-well plate and incubated for 24 h. On the next day, the tested compounds were dissolved in DMSO and added to the wells. DMSO was used as the vehicle control. After 24 h of incubation at 37 °C, 20 μl of MTT solution was added to each well and the plates were incubated for 2 h. The purple formazan formed was dissolved by the addition of 100 μl of DMSO to each well. Absorbance at 580 nm was measured and recorded using a 96-well microplate reader. The potency of cell growth inhibition for each test agent was expressed as an IC_{50} value, which defined as the concentration that caused 50% inhibition of cell growth.

3.9 Cell invasion study

The BD BioCoat™ Matrigel™ invasion chamber (BD Biosciences) was used according to the manufacturer's instructions. Compounds were dissolved in cell media at the desired concentration and dissolved in Matrigel. Twenty-five thousand of prostate cancer cells (PC-3) in serum free media were then seeded in the top chamber of the two-chamber Matrigel system. To the lower compartment, RPMI/5% FCS was added as chemoattractant. Cells were allowed to invade for 24 h. After incubation, non-invading cells were removed from the upper surface and cells on the lower surface were fixed and stained with Diff-Quik kit (BD Biosciences). Membranes were photographed and the invading cells were counted under a light microscope. Mean values from three independent assays were calculated.

4. Conclusion

The present study has shown that these metal complexes with biologically active Schiff base ligand offer an access to multi-targeted anticancer drugs, where most of the observed biological activities are metal-dependent. It is noteworthy that metal ions play a vital role in enhancing the biological activity of these complexes. Cu(II) complex **2** exhibited the strongest topo I inhibition activity, DNA cleavage, and cytotoxicity, while Zn(II) complex **1** showed better DNA binding activity, whereas Ni(II) complex **3** possesses greater anti-invasion activity. The report of Zn(II), Cu(II), and Ni(II) complexes with antimetastatic property is rare in the literature. Furthermore, the outstanding anti-metastatic property of the Ni(II) complex in contrast to its cytotoxicity has convinced us that the fate of a compound should not be only dictated by its cytotoxicity.

Acknowledgements

The authors would like to thank MOHE (FRGS-FP016-2013A, UM.C/625/1/HIR/247, PPP-PG007-2012B) for supporting this study. We would like to thank Prof. Wong C.S. and Prof. Norhanom W. for the use of their facilities.

References

1 M. L. Rothenberg, *Ann. Oncol.*, 1997, **8**, 837–855.
2 H. L. Seng, S. T. Von, K. W. Tan, M. J. Maah, S. W. Ng, R. N. Z. R. A. Rahman, I. Caracelli and C. H. Ng, *BioMetals*, 2010, **23**, 99–118.
3 Y. C. Liu, Z. F. Chen, L. M. Liu, Y. Peng, X. Hong, B. Yang, H. G. Liu, H. Liang and C. Orvig, *Dalton Trans.*, 2009, 10813–10823.
4 B. M. Zeglis, V. Divilov and J. S. Lewis, *J. Med. Chem.*, 2011, **54**, 2391–2398.
5 D. Palanimuthu, S. V. Shinde, K. Somasundaram and A. G. Samuelson, *J. Med. Chem.*, 2013, **56**, 722–734.
6 P. Katkar, A. Coletta, S. Castelli, G. L. Sabino, R. A. A. Couto, A. M. Da Costa Ferreira and A. Desideri, *Metallomics*, 2014, **6**, 117–125.
7 K. W. Tan, H. L. Seng, F. S. Lim, S. C. Cheah, C. H. Ng, K. S. Koo, M. R. Mustafa, S. W. Ng and M. J. Maah, *Polyhedron*, 2012, **38**, 275–284.
8 M. C. Rodrìguez-Argüelles, M. B. Ferrari, F. Bisceglie, C. Pelizzi, G. Pelosi, S. Pinelli and M. Sassi, *J. Inorg. Biochem.*, 2004, **98**, 313–321.
9 D. M. Kong, J. Wang, L. N. Zhu, Y. W. Jin, X. Z. Li, H. X. Shen and H. F. Mi, *J. Inorg. Biochem.*, 2008, **102**, 824–832.
10 A. Silvestri, G. Barone, G. Ruisi, D. Anselmo, S. Riela and V. T. Liveri, *J. Inorg. Biochem.*, 2007, **101**, 841–848.
11 G. Barone, N. Gambino, A. Ruggirello, A. Silvestri, A. Terenzi and V. T. Liveri, *J. Inorg. Biochem.*, 2009, **103**, 731–737.
12 S. T. Chew, K. M. Lo, S. K. Lee, M. P. Heng, W. Y. Teoh, K. S. Sim and K. W. Tan, *Eur. J. Med. Chem.*, 2014, **76**, 397–407.
13 S. K. Lee, K. W. Tan, S. W. Ng, K. K. Ooi, K. P. Ang and M. A. Abdah, *Spectrochim. Acta, Part A*, 2014, **121**, 101–108.
14 A. Masta, P. J. Gray and D. R. Phillips, *Nucleic Acids Res.*, 1995, **23**, 3508–3515.
15 E. S. Newlands, M. F. G. Stevens, S. R. Wedge, R. T. Wheelhouse and C. Brock, *Cancer Treat. Rev.*, 1997, **23**, 35–61.
16 U. Schatzschneider and J. K. Barton, *J. Am. Chem. Soc.*, 2004, **126**, 8630–8631.
17 P. Zabierowski, J. Szklarzewicz, K. Kurpiewska, K. Lewiński and W. Nitek, *Polyhedron*, 2013, **49**, 74–83.
18 L. Z. Li, C. Zhao, T. Xu, H. W. Ji, Y. H. Yu, G. Q. Guo and H. Chao, *J. Inorg. Biochem.*, 2005, **99**, 1076–1082.
19 A. A. El-Sherif and T. M. A. Eldebss, *Spectrochim. Acta, Part A*, 2011, **79**, 1803–1814.
20 G. Grivani, A. D. Khalaji, V. Tahmasebi, K. Gotoh and H. Ishida, *Polyhedron*, 2012, **31**, 265–271.
21 L. Casella and M. Gullotti, *J. Am. Chem. Soc.*, 1981, **103**, 6338–6347.
22 A. M. Farag, T. S. Guan, H. Osman, A. M. S. A. Majid, M. A. Iqbal and M. B. K. Ahamed, *Med. Chem. Res.*, 2013, **22**, 4727–4736.
23 A. Haikarainen, J. Sipilä, P. Pietikäinen, A. Pajunen and I. Mutikainen, *J. Chem. Soc., Dalton Trans.*, 2001, 991–995.
24 D. M. Boghaei and E. Askarizadeh, *J. Coord. Chem.*, 2008, **61**, 1917–1926.
25 A. W. Williamson, *Q. J., Chem. Soc.*, 1852, **4**, 229–239.
26 V. Bethmont, F. Fache and M. Lemaire, *Tetrahedron Lett.*, 1995, **36**, 4235–4236.
27 S. Saha, R. K. Kottalanka, P. Bhowmik, S. Jana, K. Harms, T. K. Panda, S. Chattopadhyay and H. P. Nayek, *J. Mol. Struct.*, 2014, **1061**, 26–31.
28 D. B. Yadav, G. L. Morgans, B. A. Aderibigbe, L. G. Madeley, M. A. Fernandes, J. P. Michael, C. B. De Koning and W. A. L. Van Otterlo, *Tetrahedron*, 2011, **67**, 2991–2997.
29 B. Basavaraju, H. S. Bhojya Naik and M. C. Prabhakara, *Bioinorg. Chem. Appl.*, 2007, **2007**, 36497.
30 K. Samanta, B. Chakravarti, J. K. Mishra, S. K. D. Dwivedi, L. V. Nayak, P. Choudhry, H. K. Bid, R. Konwar, N. Chattopadhyay and G. Panda, *Bioorg. Med. Chem. Lett.*, 2010, **20**, 283–287.
31 P. A. Duckworth, F. S. Stephens, K. P. Wainwright, K. D. V. Weerasuria and S. B. Wild, *Inorg. Chem.*, 1989, **28**, 4531–4535.
32 A. Werner, *Z. Anorg. Allg. Chem.*, 1893, **3**, 267–330.
33 B. J. Coe and S. J. Glenwright, *Coord. Chem. Rev.*, 2000, **203**, 5–80.
34 X. Sheng, X. M. Lu, J. J. Zhang, Y. T. Chen, G. Y. Lu, Y. Shao, F. Liu and Q. Xu, *J. Org. Chem.*, 2007, **72**, 1799–1802.
35 N. Shahabadi, S. Kashanian and F. Darabi, *Eur. J. Med. Chem.*, 2010, **45**, 4239–4245.
36 J. Hernandez-Gil, S. Ferrer, E. Salvador, J. Calvo, E. Garcia-Espana and J. C. Mareque-Rivas, *Chem. Commun.*, 2013, **49**, 3655–3657.
37 M. W. Göbel, J. W. Bats and G. Dürner, *Angew. Chem., Int. Ed.*, 1992, **31**, 207–209.
38 U. Scheffer, A. Strick, V. Ludwig, S. Peter, E. Kalden and M. W. Göbel, *J. Am. Chem. Soc.*, 2005, **127**, 2211–2217.
39 C. Li, F. Zhao, Y. Huang, X. Liu, Y. Liu, R. Qiao and Y. Zhao, *Bioconjugate Chem.*, 2012, **23**, 1832–1837.
40 S. S. Tonde, A. S. Kumbhar, S. B. Padhye and R. J. Butcher, *J. Inorg. Biochem.*, 2006, **100**, 51–57.
41 P. U. Maheswari, S. Roy, H. Den Dulk, S. Barends, G. Van Wezel, B. Kozlevčar, P. Gamez and J. Reedijk, *J. Am. Chem. Soc.*, 2006, **128**, 710–711.
42 H. L. Seng, H. K. A. Ong, R. N. Z. R. A. Rahman, B. M. Yamin, E. R. T. Tiekink, K. W. Tan, M. J. Maah, I. Caracelli and C. H. Ng, *J. Inorg. Biochem.*, 2008, **102**, 1997–2011.
43 P. A. N. Reddy, M. Nethaji and A. R. Chakravarty, *Eur. J. Inorg. Chem.*, 2004, 1440–1446.
44 S. Anbu, M. Kandaswamy and B. Varghese, *Dalton Trans.*, 2010, 3823–3832.
45 N. H. Khan, N. Pandya, K. J. Prathap, R. I. Kureshy, S. H. R. Abdi, S. Mishra and H. C. Bajaj, *Spectrochim. Acta, Part A*, 2011, **81**, 199–208.
46 R. Eshkourfu, B. Čobeljić, M. Vujčić, I. Turel, A. Pevec, K. Sepčić, M. Zec, S. Radulović, T. Srdić-Radić, D. Mitić, K. Andjelković and D. Sladić, *J. Inorg. Biochem.*, 2011, **105**, 1196–1203.
47 P. Tamil Selvi, H. Stoeckli-Evans and M. Palaniandavar, *J. Inorg. Biochem.*, 2005, **99**, 2110–2118.

48 B. L. Fei, W. S. Xu, H. W. Tao, W. Li, Y. Zhang, J. Y. Long, Q. B. Liu, B. Xia and W. Y. Sun, *J. Photochem. Photobiol., B*, 2014, **132**, 36–44.
49 J. B. Lepecq and C. Paoletti, *J. Mol. Biol.*, 1967, **27**, 87–106.
50 A. E. Friedman, J. C. Chambron, J. P. Sauvage, N. J. Turro and J. K. Barton, *J. Am. Chem. Soc.*, 1990, **112**, 4960–4962.
51 K. E. Erkkila, D. T. Odom and J. K. Barton, *Chem. Rev.*, 1999, **99**, 2777–2796.
52 D. H. Tjahjono, S. Mima, T. Akutsu, N. Yoshioka and H. Inoue, *J. Inorg. Biochem.*, 2001, **85**, 219–228.
53 G. Barone, A. Terenzi, A. Lauria, A. M. Almerico, J. M. Leal, N. Busto and B. García, *Coord. Chem. Rev.*, 2013, **257**, 2848–2862.
54 P. Feng, T. L. Li, Z. X. Guan, R. B. Franklin and L. C. Costello, *Prostate*, 2002, **52**, 311–318.
55 R. B. Franklin and L. C. Costello, *Arch. Biochem. Biophys.*, 2007, **463**, 211–217.
56 T. D. Pfister, W. C. Reinhold, K. Agama, S. Gupta, S. A. Khin, R. J. Kinders, R. E. Parchment, J. E. Tomaszewski, J. H. Doroshow and Y. Pommier, *Mol. Cancer Ther.*, 2009, **8**, 1878–1884.
57 K. Lang, T. L. Drell Iv, K. S. Zaenker and F. Entschladen, *Recent Pat. Anti-Cancer Drug Discovery*, 2006, **1**, 69–80.
58 S. Das, S. Sinha, R. Britto, K. Somasundaram and A. G. Samuelson, *J. Inorg. Biochem.*, 2010, **104**, 93–104.
59 D. A. Medvetz, K. D. Stakleff, T. Schreiber, P. D. Custer, K. Hindi, M. J. Panzner, D. D. Blanco, M. J. Taschner, C. A. Tessier and W. J. Youngs, *J. Med. Chem.*, 2007, **50**, 1703–1706.
60 V. Kolenko, E. Teper, A. Kutikov and R. Uzzo, *Nat. Rev. Urol.*, 2013, **10**, 219–226.
61 H. N. Keer, F. D. Gaylis, J. M. Kozlowski, H. C. Kwaan, K. D. Bauer, A. A. Sinha and M. J. Wilson, *Prostate*, 1991, **18**, 201–214.
62 A. Levina, A. Mitra and P. A. Lay, *Metallomics*, 2009, **1**, 458–470.
63 A. Bergamo and G. Sava, *Dalton Trans.*, 2007, 1267–1272.
64 M. Zec, T. Srdic-Rajic, A. Konic-Ristic, T. Todorovic, K. Andjelkovic, I. Filipovic-Ljeskovic and S. Radulovic, *Anti-Cancer Agents Med. Chem.*, 2012, **12**, 1071–1080.
65 G. M. Sheldrick, *Acta Crystallogr., Sect. A: Found. Crystallogr.*, 2007, **64**, 112–122.
66 L. J. Barbour, *J. Supramol. Chem.*, 2001, **1**, 189–191.
67 W. Xu, X. Yang, L. Yang, Z. L. Jia, L. Wei, F. Liu and G. Y. Lu, *New J. Chem.*, 2010, **34**, 2654–2661.
68 L. Liu, G.-M. Zhang, R.-G. Zhu, Y.-H. Liu, H.-M. Yao and Z.-B. Han, *RSC Adv.*, 2014, **4**, 46639–46645.
69 C. K. Mirabelli, C. H. Huang and S. T. Crooke, *Cancer Res.*, 1980, **40**, 4173–4177.
70 R. P. Hertzberg and P. B. Dervan, *J. Am. Chem. Soc.*, 1982, **104**, 313–315.
71 A. M. Pyle, J. P. Rehmann, R. Meshoyrer, C. V. Kumar, N. J. Turro and J. K. Barton, *J. Am. Chem. Soc.*, 1989, **111**, 3051–3058.
72 A. Wolfe, G. H. Shimer Jr and T. Meehan, *Biochemistry*, 1987, **26**, 6392–6396.

